J Mol Model (2011) 17:1227–1239
DOI 10.1007/s00894-010-0804-7

ORIGINAL PAPER

Electronic structure and conformational properties of *1H*-indole-3-acetic acid

María C. Pérez Schmit · Alicia H. Jubert · Arturo Vitale · Rosana M. Lobayan

Received: 15 April 2010 / Accepted: 7 July 2010 / Published online: 13 August 2010

Abstract The conformational space of *1H*-Indole-3-Acetic Acid (IAA) was scanned using molecular dynamics at semiempirical level, and complemented with functional density calculations at B3LYP/6-31G** level, 14 conformers of lowest energy were obtained. Electronic distributions were analyzed at a higher calculation level, thus improving the basis set (B3LYP/6-311++G**). A topological study based on Bader's theory (AIM: atoms in molecules) and natural bond orbital (NBO) framework performed with the aim to analyze the stability and reactivity of the conformers allowed the understanding of electronic aspects relevant in the study of the antioxidant properties of IAA. Intramolecular hydrogen bonds were found and were characterized as blue-shifting hydrogen bonding interactions. Furthermore, molecular electrostatic potential maps (MEPs) were obtained and analyzed in the light of AIM and NBO results, thus showing subtle but essential features related not only to reactivity but also with intramolecular weak interactions, charge delocalization and structure stabilization.

Keywords Atoms in molecules (AIM theory) · Density functional theory · 1H-indole-3-acetic acid (IAA) · Maps of electrostatic potential · Natural bond orbital analysis · Topological properties

Electronic supplementary material The online version of this article (doi:10.1007/s00894-010-0804-7) contains supplementary material, which is available to authorized users.

M. C. Pérez Schmit · R. M. Lobayan (✉)
Facultad de Ingeniería, Universidad de la Cuenca del Plata,
Lavalle 50,
3400 Corrientes, Argentina
e-mail: rlobayan@ucp.edu.ar

A. H. Jubert
CEQUINOR Facultad de Ciencias Exactas y Facultad de Ingeniería, Universidad Nacional de La Plata,
CC 962,
1900 La Plata, Argentina

A. Vitale
PRALIB (UBA, CONICET), Facultad de Farmacia y Bioquímica,
Universidad de Buenos Aires,
Junín 956,
C1113AAD Buenos Aires, Argentina

Introduction

Indole derivatives are biologically important chemicals present in microorganisms, plants, and animals [1], and represent an important class of therapeutical agents in medicinal chemistry. Indolic compounds are very efficient antioxidants, protecting both lipids and proteins from peroxidation, and it is known that the Indole structure influences the antioxidant efficacy in biological systems [2-5].

Radical scavenging by indolic compounds is strongly modulated by their functional residues. All indolamines have a heteroaromatic ring system of high electroreactivity and they only differ in the functional group in their side chain. These substituents determine to a great extent the reactivity, potency, and efficiency of radical scavenging activity [6].

Due to the free radical scavenger and antioxidant properties of Indole derivatives, it is of paramount importance to explore deeply the stereoelectronic aspects that would be relevant in the study of their stabilization and antioxidant activities.

The aim of this work is to analyze the geometric and electronic properties of IAA conformers, thus performing a complete search on the conformational space. A deeper

study of the possible hydrogen bonding interactions and the structural and electronic factors relevant in their stability and reactivity were also performed. To the best of our knowledge this kind of analysis is not shown in the literature.

The conformational space of these molecules was scanned using molecular dynamics (MD) calculations, and complemented with density functional calculations at the B3LYP level with a 6-31G** basis set to optimize the geometry of the lowest-energy conformers as obtained in the simulations.

A rigorous approach based in Bader's atoms in molecules (AIM) theory to detect and characterize hydrogen bond interactions [7-9], together with natural bond orbital (NBO) analysis were also used [10].

Molecular electrostatic potential maps (MEPs) were obtained and analyzed in the light of AIM and NBO results. The results reported contribute to the understanding of the structure, stability and reactivity of IAA and others Indole derivatives.

Computational details

Conformational space of the IAA molecules was studied using the MD module of the HyperChem package [11]. With the aid of the MM+ force field several simulations were accomplished. The starting geometries were heated from 0 to 800 K in 0.1 ps. Then, the temperature was kept constant by coupling the system to a simulated thermal bath with a bath relaxation time of 0.5 ps. The simulation time step was 0.5 fs. After an equilibration period of 1 ps a 500 ps-long simulation was run saving the coordinates every 1 ps. Those geometries were then optimized to an energy gradient less than 0.01 kcalmol^{-1} $Å^{-1}$ at a semiempirical level (AM1).

The lowest-energy conformers of the molecules, obtained according to the above methodology were further studied by the density functional theory as implemented by the Gaussian 03 package [12]. Geometry optimizations were performed using the Becke three parameter hybrid functional [13] with the Lee-Yang-Parr correlation functional [14], a combination that gives rise to the well known B3LYP method. For all the atoms a 6-31G** basis set was used.

The topological analysis and evaluation of local properties were performed with the PROAIM software [15] using the wave functions calculated at the B3LYP level and the improved 6-311++G** basis set. An NBO analysis at the same level was performed [10].

Vibrational analysis at the same level of theory as above for all optimized geometries was performed in order to verify whether they are minima on the hypersurface of potential energy of the molecule. MEPs were calculated with the Gaussian package, and visual representations were obtained with the Molekel program [16].

Results and discussion

Geometrical and conformational analysis of IAA

The backbone of IAA consists of a heteroaromatic planar Indole ring and an acetyl side chain (at position 3) that can adopt several distinct orientations with respect to the ring defined by three dihedral angles (δ_1: C_2—C_3—C_8—C_9, δ_2: C_3—C_8—C_9—O_{10}, δ_3: C_8—C_9—O_{11}—H) (Fig. 1). Variations can give rise to several different conformers. Through the study of the conformational space in vacuum we found 14 lowest energy conformers with symmetry C_1, which in stability order are: a) CCT, b) A^+A^+T/A^-A^-T, c) A^+A^-T/A^-A^+T, d) A^+CT/A^-CT, e) G^+A^+T /G^-A^-T, A^+TC/A^-TC, f) CCC, and g) A^+CC/A^-CC (see Fig. 2). They were named according to IUPAC recommendations [17], and were confirmed by absence of imaginary frequencies in the vibrational analysis.

Six pairs of them account for structures of the same energy, but differing in the orientation of the acetyl group with respect to the plane of the Indole ring: one of them with the acetyl moiety upward oriented, *Re*-face, and the other isomer having the acetyl moiety downward oriented, *Si*-face. Each pair shows torsion angles of opposite sign, Table 1. Due to the similarity of the corresponding electronic distribution we will study only one conformer of each pair, selecting the conformation in which the acetyl moiety is upward oriented (*Re* isomers).

Two conformers (A^+CT and A^-CT) were not detected by direct MD procedure; they arose broadening the conformational search on systematic way.

The second most stable conformer, A^+A^+T, differs from the most stable form in the δ_1 and δ_2 axis, whose values are

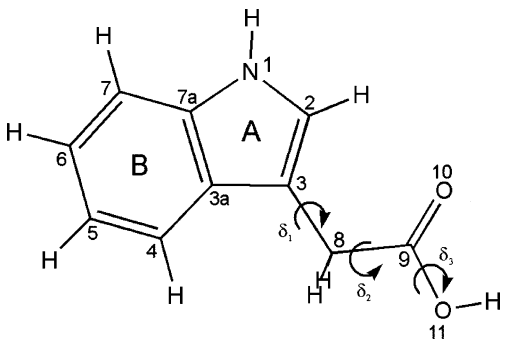

Fig. 1 Heteroaromatic planar Indole ring and an acetyl side chain of IAA backbone. Dihedral angles (δ_1: C_2—C_3—C_8—C_9, δ_2: C_3—C_8—C_9—O_{10}, δ_3: C_8—C_9—O_{11}—H) defines distinct orientations of acetyl side chain with respect to the ring

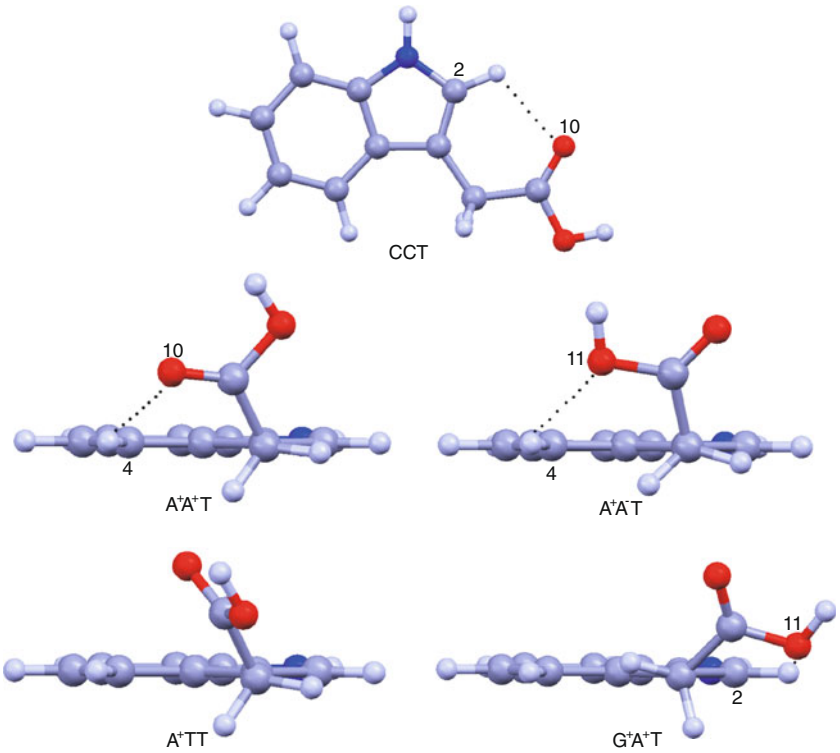

Fig. 2 Five most stable conformers of IAA monomer. According to IUPAC recommendations the first letter characterizes the orientation of the C_9 atom relative to the central C_3—C_8 bond, the second letter describes the C_3—C_8—C_9—O_{10} angle, and the third letter specifies the orientation of the H relative to the central C_9—O_{11}. Dotted lines: Intramolecular hydrogen bond interactions

115.7° and 95.7°, assuming an anticlinal configuration. These two conformers differ in energy in 0.75 kcal mol^{-1}. The third most stable conformer is A^+A^-T, which differs from CCT in the δ_1 and δ_2 dihedral angles, 102.3° and -92.6°. They assume an anticlinal configuration. In conformer A^+CT, the values for the dihedral angles mentioned above are 116.6° and 16.8°. The G^+A^+T conformer differs from the most stable in the angles δ_1 and δ_2, which assume a clinal and anticlinal configuration, respectively. Geometrical parameters of the other conformers are also shown in Table 1.

Other relevant parameters for conformers are displayed in Table 2. The geometrical features suggest the following intramolecular hydrogen bonding interactions: $O_{10}\cdots H_2$ (CCT), $O_{10}\cdots H_4$ (A^+A^+T), $O_{11}\cdots H_4$ (A^+A^-T), and $O_{11}\cdots H_2$ (G^+A^+T) (cf. Fig. 2). In all of them the proton donor atom (D) is a carbon atom and the oxygen atom acts as the proton acceptor (A) in a A···H—D interaction.

In CCT, A^+A^+T, A^+A^-T and G^+A^+T the intramolecular distances O···H around 2.363-2.752 Å, in the expected range of 2.2-3.2 Å for A···H distance[18] (see Table 2). Another parameter that characterizes a hydrogen bond is the distance between the C atom attached to the hydrogen of the bridge, and the oxygen atom. This distance is between 2.904-3.466 Å in agreement with expected values (3.2-4.0 Å for D···A distance [18]). The bond angle between donor and acceptor atoms varies in the range of 104.0-124.5° (expected D—H···A angles about 90-150°) [18], thus showing the donor directionality associated with the suggested H-bonds. The C_2—H bond length in CCT and G^+A^+T is shorter (≈ 0.003 Å) than in A^+A^+T, A^+A^-T and A^+CT. In A^+A^+T, A^+A^-T and A^+CT a similar behavior in C_4—H bond length can be observed.

Topology of the electronic charge density

AIM theory is based on the analysis of critical points (CPs) of the molecular charge density, ρ. At these points, the gradient of the electronic density, ∇ρ, is null, and it is characterized by the three eigenvalues, λ_i (i=1, 2, 3), of the $\nabla^2\rho$ Hessian matrix. The CPs were named and classified as (r, s) according to their rank, r (number of non-zero eigenvalues), and signature, s (the three eigenvalues algebraic sum).

Several properties evaluated at the bond CP (BCP) (a (3,-1) CP) constitute powerful tools to classify a given chemical structure [19]. Interactions attributable to covalent or polarized bonds are characterized by large ρ_b values, $\nabla^2\rho_b<0$, $|\lambda_1|/\lambda_3>1$ and $G_b/\rho_b<1$ at BCP. Interactions classified as closed shell, typical of highly ionic bonds, hydrogen bonds, and van der Waals interactions, are described by relatively low ρ_b values, $\nabla^2\rho_b>0$, $|\lambda_1|/\lambda_3<1$ and $G_b/\rho_b<1$. Another interesting parameter is the ellipticity, ε, defined as λ_1/λ_2-1. Ellipticity measures the extent to

Table 1 Relevant internal coordinates of lowest energy conformers of IAA calculated at B3LYP/6-31G** level

First lowest energy conformers	CCT	A^+A^+T	A^-A^-T	A^+A^-T	A^-A^+T	A^+CT	A^-CT	G^+A^+T	G^-A^-T	Other conformers	A^+TC	A^-TC	CCC	A^+CC	A^-CC
ΔE (kcalmol^{-1})	0	0.75	0.75	0.94	0.94	1.2	1.2	1.72	1.72		3.36	3.36	5.6	6.98	6.98
Dihedral angle (°)															
$C_2—C_3—C_8—C_9$	0	115.7	-115.7	102.3	-102.3	116.6	-116.4	46.6	-46.6		106	-106.1	0	110.6	-110.8
$C_3—C_8—C_9—O_{10}$	0	95.7	-95.6	-92.6	92.8	16.8	-15.5	109.8	-109.8		157.4	-157.3	0	-4.4	4.4
$C_8—C_9—O_{11}—H$	180	177.2	-177.2	-176.6	176.6	-177.7	177.9	178.7	178.7		5.7	-5.7	0	-0.9	0.9

Table 2 Others relevant geometrical parameters obtained of the lowest energy IAA conformers calculated at the B3LYP/6-31G** level

	Conformers				
	CCT	A^+A^+T	A^+A^-T	A^+CT	G^+A^+T
Distances (Å)					
$C_9—O_{10}$	1.212	1.212	1.210	1.209	1.209
$C_9—O_{11}$	1.357	1.355	1.357	1.359	1.361
$O_{11}—H$	0.972	0.972	0.972	0.972	0.972
$C_4—H$	1.087	1.085	1.085	1.085	1.087
$C_2—H$	1.078	1.081	1.081	1.081	1.080
$O_{10}\cdots H_2$ ($O_{10}\cdots C_2$)	2.363 (2.904)				
$O_{10}\cdots H_4$ $O_{10}\cdots C_4$		2.734 (3.466)		2.939 (3.370)	
$O_{11}\cdots H_4$ ($O_{11}\cdots C_4$)			2.752 (3.392)		
$O_{11}\cdots H_2$ ($O_{11}\cdots C_2$)					2.605 (3.073)
Angles (°)					
$C_9—O_{10}\cdots H_2$	107.0				
$C_9—O_{10}\cdots H_4$		97.6		92.5	
$C_9—O_{11}\cdots H_4$			108.8		
$C_9—O_{11}\cdots H_2$					99.0
$O_{10}\cdots H—C_2$	109.4				
$O_{10}\cdots H—C_4$		124.5		104.0	
$O_{11}\cdots H—C_4$			117.5		
$O_{11}\cdots H—C_2$					105.4
$O_{11}—C_9—O_{10}$	121.9	122.5	122.5	122.4	122.1

which density is preferentially accumulated in a given plane containing the bond path. If $\lambda_1=\lambda_2$, then $\varepsilon=0$, and the bond is cylindrically symmetric, e.g., a C—C single bond in ethane, and a triple bond in acetylene [9].

A (3,-3) critical point is a maximum in all directions, and as often coincides with the nucleus position is called nuclear attractor or nuclear critical point (NCP). In this work we show that properties evaluated at this point are useful tools to analyze the behavior of electronic distribution.

Table 3 shows the most significant topological local properties at BCPs for CCT conformer. The electron charge density (ρ_b), the Laplacian of the electron charge density ($\nabla^2\rho_b$), the three eigenvalues of the Hessian matrix (λ_1, λ_2 and λ_3), the ellipticity (ε), the relationship between perpendicular and parallel curvatures ($|\lambda_1|/\lambda_3$), and the kinetic energy density per charge unit (G_b/ρ_b), for all chemical bonds of the lowest energy conformers obtained. As supplementary material, these topological parameters are also shown for A^+A^+T, A^+A^-T, A^+CT and G^+A^+T conformers that comprise the conformational space (Tables S1a to d).

At C—C, C—N, N—H and C—H bonds of the rings A and B and the acetyl moiety high ρ_b values, $|\lambda_1|/\lambda_3>1$ and

Table 3 Topological properties at bond critical points (BCPs) (3, -1) in the CCT conformer calculated at the B3LYP/6-311++G** level of theory[a]

	Bond	Bond length	ρ_b	$\nabla^2\rho_b$	λ_1	λ_2	λ_3	ε	G_b/ρ_b	$\lvert\lambda_1\rvert/\lambda_3$
Ring A	C_{7a}—N_1	1.379	0.301	-0.740	-0.602	-0.538	0.399	0.119	0.753	1.507
	N_1—C_2	1.383	0.297	-0.699	-0.587	-0.518	0.406	0.133	0.785	1.445
	C_2—C_3	1.373	0.319	-0.876	-0.684	-0.506	0.314	0.352	0.377	2.178
	C_3—C_{3a}	1.443	0.280	-0.698	-0.563	-0.478	0.343	0.178	0.304	1.640
	C_{3a}—C_{7a}	1.422	0.299	-0.809	-0.629	-0.523	0.343	0.201	0.310	1.833
	N_1—H	1.006	0.341	-1.669	-1.305	-1.242	0.877	0.051	0.152	1.488
	C_2—H	1.078	0.288	-1.018	-0.806	-0.776	0.563	0.039	0.117	1.430
	C_3—C_8	1.500	0.252	-0.601	-0.489	-0.461	0.348	0.060	0.233	1.403
Ring B	C_{3a}—C_4	1.406	0.300	-0.817	-0.621	-0.524	0.329	0.185	0.313	1.890
	C_4—C_5	1.390	0.310	-0.856	-0.652	-0.528	0.323	0.236	0.336	2.017
	C_5—C_6	1.409	0.299	-0.810	-0.621	-0.520	0.332	0.193	0.313	1.872
	C_6—C_7	1.390	0.309	-0.851	-0.649	-0.524	0.322	0.237	0.336	2.013
	C_7—C_{7a}	1.398	0.304	-0.838	-0.637	-0.524	0.323	0.215	0.324	1.971
	C_4—H	1.087	0.279	-0.949	-0.740	-0.724	0.514	0.022	0.140	1.439
	C_5—H	1.086	0.280	-0.953	-0.743	-0.725	0.515	0.025	0.140	1.443
	C_6—H	1.086	0.280	-0.956	-0.745	-0.728	0.517	0.023	0.139	1.441
	C_7—H	1.086	0.278	-0.944	-0.737	-0.719	0.512	0.025	0.141	1.440
Acetyl moiety	C_8—C_9	1.513	0.255	-0.620	-0.510	-0.470	0.360	0.085	0.239	1.418
	C_9—O_{10}	1.212	0.415	-0.285	-1.098	-1.015	1.829	0.081	1.530	0.601
	C_9—O_{11}	1.357	0.296	-0.512	-0.640	-0.623	0.750	0.027	0.998	0.853
	O_{11}—H	0.972	0.356	-2.475	-1.757	-1.726	1.008	0.018	0.186	1.743
	C_8—H_a	1.099	0.271	-0.889	-0.708	-0.694	0.513	0.019	0.152	1.379
	C_8—H_b	1.099	0.271	-0.889	-0.707	-0.694	0.513	0.019	0.152	1.379

[a] ρ_b,$\nabla^2\rho_b$, G_b/ρ_b, λ_1, λ_2 , λ_3 are expressed in a.u. and bond lengths in Å

$G_b/\rho_b<1$, important and less than zero Laplacian was found for all studied conformers, and therefore all of them can be characterized as covalent interactions. A detailed description of the topological properties of C—C bonds and the comparison with the Indole parent compound is given as supplementary material (values for Indole in Table S1e).

The increase of ε in A rings both in IAA and in Indole shows a π-enriched ring A, moreover the π-character of these bonds increase in the ring A of IAA with respect to Indole. The mechanisms underlying this feature will be analyzed below through a NBO analysis, thus showing the importance of charge transferences related to the acetyl side chain.

The topological characterization of C_{7a}—N_1 slightly differed from topological features of N_1—C_2. Our findings indicate that the acetyl side chain has a slight effect on C—N bonds and do not affect the N_1—H bond (see supplementary material for a detailed discussion).

Analyzing C—H bonds, the C_4—H bond length changed with respect to Indole: a shortening (0.001 Å) in A^+A^+T, A^+A^-T, and AC^+T was found. Consequently an increase of ρ_b and $\nabla^2\rho_b$ was found (see Table 3, S1a, b, c and d). The C_2—H bond showed an increase of ρ_b and $\nabla^2\rho_b$ in CCT and G^+A^+T with respect to the Indole and other conformers which is in agreement to the slight shortening in their bond length. These results are related to intramolecular H-bonds and will be further analyzed below.

Along the conformational space of IAA C_8—H_a and C_8—H_b bonds showed changes in bond lengths and topological parameters (see Table 3, S1a, b, c and d). High symmetry in CCT was found; both C_8—H_a and C_8—H_b showed similar geometrical and topological parameters. In A^+A^+T and A^+A^-T C_8—H_a and C_8—H_b bonds showed only a slight symmetry. In CCT we found the weaker interactions, in A^+A^+T and A^+A^-T we found the strongest ones and in G^+A^+T and A^+CT one of them is strong and the other is weak. When the values of charge density at BCPs decrease their bond lengths increase. All these findings will be related to charge delocalization through NBO analysis and MEPs.

The BCPs of C_9—O_{10} and C_9—O_{11} showed values of an intermediate or shared polar covalent bond (high ρ_b, important and less than zero $\nabla^2\rho_b$, $|\lambda_1|/\lambda_3<1$, and $G_b/\rho_b>1$). This attribute obeys the increase in positive eigenvalue of the Hessian matrix (Table 3) and indicates an increase in the contraction extent of ρ_b parallel to the bond and from CP toward each of the neighboring nuclei.

In agreement with the geometrical features mentioned above (Table 2), the AIM analysis allowed us to identify the formation of intramolecular hydrogen bonding interactions. Local topological properties calculated in the respective BCP and RCP are displayed in Table 4. The intramolecular hydrogen bonding interactions characterized by AIM in conformers were: a) $O_{10}\cdots H—C_2$ (CCT), b) $O_{10}\cdots H—C_4$ (A^+A^+T), c) $O_{11}\cdots H—C_4$ (A^+A^-T), d) $O_{11}\cdots H—C_2$ (G^+A^+T). The formation of these H-bonds closes six-membered (in (a) and (d)), and seven-membered (in (b) and (c)) rings respectively and are accompanied by the appearance of ring critical points (RCPs), as required to fulfill the Poincaré-Hopf relationship [7]. All these particular interactions were described by relatively low ρ_b values, $\nabla^2\rho_b>0$, $|\lambda_1|/\lambda_3<1$ and $G_b/\rho_b<1$. They are classified as closed shell. In A^+CT monomer, intramolecular hydrogen bondings were not found through AIM search.

In agreement with previous results for intramolecular hydrogen bonding interactions (density values between 0.002−0.034 a.u., and $\nabla^2\rho_b$ values between 0.016−0.139 a.u. [20]) the electronic charge density values at H-bond CPs were in the range of 0.006 to 0.014 a.u. and the Laplacian values at the same point were in the range of 0.020 to 0.051 a.u..

The hydrogen bonding interaction in CCT is the strongest (d=2.363 Å; ρ_b=0.014 a.u.; $\nabla^2\rho_b$ = 0.051 a.u.; ε=0.223). In fact, in this conformer the density value at H-bond CP was one order of magnitude higher than that corresponding to the other conformers, according to the shortening of the O···H distance. The G^+A^+T showed a ρ_b value of 0.009 a.u. at H-bond CP ($O_{11}\cdots H_2$) slightly higher than A^+A^+T and A^+A^-T (see Table 4). However, the interaction is associated with the highest ellipticity value (ε=0.560). The ellipticity value is not only a measure of the π-character of a bond, but also is a measure of the structure stability. In fact, high ellipticity values reflect structural instability [20]. Therefore our results show that $O_{11}\cdots H_2$ bond in G^+A^+T can be easily broken despite their higher CP density.

The shortening of the C_2—H bond length in CCT and G^+A^+T, reported above, can be related with their donor role in $C_2—H\cdots O_{10}$ (CCT) and $C_2—H\cdots O_{11}$ (G^+A^+T) interactions. In fact, in conformers where C_2—H bond was not involved in hydrogen bonding interactions, larger bond lengths were reported. Interestingly, our infrared frequency calculations indicate that in CCT and G^+A^+T conformers the νC_2H mode appear at 3306 and 3281 cm^{-1}, respectively, while in other conformers, e.g., A^+CT, where C_2—H is not involved in H-bond, the corresponding wavenumber was 3258 cm^{-1}. Our results certify a shifting to blue frequencies of 48 and 23 cm^{-1}, in CCT and G^+A^+T respectively. These kinds of H-bonds are called blue shifted, improper or anti-H-bonds [21]. For C_4—H bond in A^+A^+T and A^+A^-T a similar behavior was found.

NBO analysis

The NBO analysis provides energies of hyperconjugative interactions from the second-order perturbation approach

$$E^{(2)} = -n_i \frac{F_{ij}^2}{\varepsilon_j - \varepsilon_i}$$

where F_{ij} is the Fock matrix element between the i and j NBO orbitals, ε_j and ε_i are the energies of i and j NBOs, and n_i is the population of the donor i orbital. Thus two main terms controlling the magnitude of a $i\rightarrow j$ hyperconjugative interaction namely: the difference in energy between the interacting orbitals (the $\Delta E = \varepsilon_j - \varepsilon_i$ term) and the magnitude of the Fock matrix element, F_{ij}, which varies in parallel to the overlap matrix element, S_{ij} [22].

In Table 5 selected NBO second-order stabilization energies, $E^{(2)}$ are shown. The charge transferences related to the electronic delocalization between Indole backbone and acetyl moiety are reported. Strongest charge delocalization in CCT was found (43.59 $kcalmol^{-1}$, 28.78 $kcalmol^{-1}$, 25.20 $kcalmol^{-1}$, 32.41 $kcalmol^{-1}$, and 31.15 $kcalmol^{-1}$ in

Table 4 Topological properties at BCP (3, -1) for hydrogen bonds in IAA conformers calculated at B3LYP/6-311++G** level of theory. Relevant topological properties at (3, +1) BCP for the corresponding rings are also reported[a]

BCP	Conformers	H-Bond	Distance A···H	ρ_b	$\nabla^2\rho_b$	λ_1	λ_2	λ_3	ε	G_b/ρ_b	$\lvert\lambda_1\rvert/\lambda_3$
(3, -1)	CCT	$O_{10}\cdots H_2$	2.363	0.014	0.051	-0.013	-0.011	0.075	0.223	0.786	0.173
	A^+A^+T	$O_{10}\cdots H_4$	2.734	0.006	0.020	-0.005	-0.004	0.028	0.193	0.667	0.179
	A^+A^-T	$O_{11}\cdots H_4$	2.752	0.006	0.021	-0.005	-0.004	0.030	0.269	0.667	0.167
	G^+A^+T	$O_{11}\cdots H_2$	2.605	0.009	0.033	-0.007	-0.005	0.044	0.560	0.778	0.159
(3, +1)	CCT	$O_{10}\cdots H_2$		0.011	0.055	-0.007	0.013	0.049	-		
	A^+A^+T	$O_{10}\cdots H_4$		0.004	0.020	-0.002	0.005	0.016	-		
	A^+A^-T	$O_{11}\cdots H_4$		0.004	0.019	-0.002	0.005	0.016	-		
	G^+A^+T	$O_{11}\cdots H_2$		0.008	0.037	-0.005	0.006	0.036	-		

[a] ρ_b,$\nabla^2\rho_b$, G_b/ρ_b, λ_1, λ_2, λ_3 are expressed in a.u. and distances in Å

Table 5 Selected NBO second-order stabilization energies, $E^{(2)}$, calculated at B3LYP/6-311++G** level of theory[a]

			CCT			A^+A^+T			A^+A^-T			A^+CT			G^+A^+T		
			$E^{(2)}$	ΔE	F_{ij}	$E^{(2)}$	ΔE	F_{ij}	$E^{(2)}$	ΔE	F_{ij}	$E^{(2)}$	ΔE	F_{ij}	$E^{(2)}$	ΔE	F_{ij}
$2n_{O10}$	σ^*_{N1-C2}	*a*	0.63	0.72	0.020	-	-	-	-	-	-	-	-	-	-	-	-
σ_{C9-O11}	σ^*_{C3-C8}	*b*	1.22	1.35	0.036	-	-	-	-	-	-	1.16	1.34	0.035	-	-	-
π_{C9-O10}	σ^*_{C8-Hb}	*c*	1.24	0.77	0.028	0.75	0.77	0.022	-	-	-	0.91	0.77	0.024	1.16	0.77	0.027
	σ^*_{C8-Ha}	*d*	1.24	0.77	0.028	-	-	-	0.64	0.77	0.020	1.40	0.76	0.029	-	-	-
σ_{C8-C9}	σ^*_{C3a-C3}	*e*	3.08	1.16	0.053	-	-	-	-	-	-	-	-	-	2.45	1.15	0.047
σ_{C3-C8}	$\sigma^*_{C3a-C7a}$	*f*	1.60	1.16	0.039	1.57	1.16	0.038	1.55	1.15	0.038	1.50	1.16	0.037	1.59	1.15	0.038
	σ^*_{C2-C3}	*g*	2.71	1.21	0.051	2.18	1.20	0.046	2.12	1.20	0.045	2.27	1.21	0.047	2.28	1.20	0.047
	σ^*_{C9-O11}	*h*	2.25	0.97	0.042	-	-	-	-	-	-	2.36	0.97	0.044	-	-	-
σ_{C2-C3}	σ^*_{C3a-C3}	*i*	2.66	1.20	0.050	2.41	1.20	0.048	2.35	1.20	0.047	2.43	1.20	0.048	2.48	1.20	0.049
	σ^*_{C3-C8}	*j*	2.18	1.11	0.044	2.00	1.11	0.042	1.94	1.11	0.041	2.09	1.12	0.043	1.84	1.10	0.040
	σ^*_{C2-H}	*k*	1.33	1.13	0.035	1.25	1.11	0.033	1.24	1.11	0.033	1.21	1.11	0.033	1.28	1.12	0.034
π_{C2-C3}	σ^*_{C8-Ha}	*l*	3.27	0.63	0.042	2.80	0.65	0.039	2.03	0.64	0.033	3.04	0.63	0.040	-	-	-
	σ^*_{C8-Hb}	*m*	3.28	0.63	0.042	-	-	-	-	-	-	-	-	-	3.26	0.64	0.042
σ_{C2-H}	σ^*_{C2-C3}	*n*	1.42	1.11	0.035	1.34	1.12	0.035	1.32	1.11	0.034	1.29	1.12	0.034	1.35	1.11	0.035
σ_{C3a-C3}	σ^*_{C2-C3}	*o*	2.42	1.21	0.049	2.29	1.21	0.047	2.24	1.21	0.047	2.35	1.21	0.048	2.35	1.21	0.048
	σ^*_{C8-C9}	*p*	1.44	0.98	0.034	-	-	-	-	-	-	-	-	-	0.75	0.99	0.025
σ_{C8-Ha}	π^*_{C2-C3}	*q*	3.49	0.55	0.042	3.07	0.54	0.039	2.14	0.54	0.033	3.31	0.54	0.041	-	-	-
σ_{C8-Hb}	π^*_{C2-C3}	*r*	3.49	0.55	0.042	-	-	-	-	-	-	-	-	-	4.02	0.54	0.045
σ_{C8-C9}	σ^*_{C2-C3}	*s*	-	-	-	1.77	1.21	0.041	1.18	1.21	0.034	1.55	1.21	0.039	-	-	-
σ_{C3-C8}	σ^*_{C9-O10}	*t*	-	-	-	1.25	1.21	0.035	1.03	1.22	0.032	-	-	-	1.69	1.22	0.041
σ_{C3a-C3}	σ^*_{C8-Hb}	*u*	-	-	-	0.81	1.03	0.026	0.73	1.03	0.025	0.86	1.02	0.027	-	-	-
σ_{C4-H}	σ^*_{C4-C5}	*v*	-	-	-	0.51	1.07	0.021	-	-	-	-	-	-	-	-	-
	$\sigma^*_{C3a-C7a}$	*w*	4.64	1.03	0.062	4.78	1.02	0.062	4.69	1.02	0.062	4.68	1.02	0.062	4.65	1.02	0.062
	Σ		43.59			28.78			25.20			32.41			31.15		

[a] All values are expressed in kcal mol^{-1} , ΔE and F_{ij} values are reported in a. u

CCT, A^+A^+T, A^+A^-T, A^+CT, and G^+A^+T respectively), which explain their higher stability.

Moreover, we can see two kinds of trends. To explain them we remark on structural characteristics which are shown to be significant in the analysis of the behavior of charge transferences. We identify two series of compounds which define similar trends: on one hand CCT and A^+CT onward "series C" (periplanar array) according as the torsion angle δ_2 ranges from 0° to ±30°, and in the other hand A^+A^+T, A^+A^-T, and G^+A^+T onward "series A" (clinal array) according as the torsion angle δ_2 ranges from ±60° to ±120° (see Fig. 3).

The transferences $\sigma_{C9—O11} \rightarrow \sigma^*_{C3—C8}$ (*b*) and $\sigma_{C3—C8} \rightarrow \sigma^*_{C9—O11}$ (*h*) are proper of series C. The values of $\delta_{C3—C8—C9—O11}$ dihedral angle (180.0° and 164.9° in CCT and A^+CT) allow to explain this result ($\delta_{C3—C8—C9—O11}$= 82.9°, 86.2°, 70.4° for A^+A^+T, A^+A^-T and G^+A^+T, respectively), thus showing an important overlap between $\sigma_{C9—O11}$ and $\sigma_{C3—C8}$ orbitals only in series C where they are antiperiplanar to each other. Moreover, the same arguments also explain the augmented second order energy in CCT with respect to A^+CT (1.22 and 1.16 kcal mol^{-1} respectively) through increased F_{ij} value, because ΔE remains unaltered. This finding can be related with an increased orbital overlap due to the increase in $\delta_{C3—C8—C9—O11}$ dihedral angle.

The transference $\sigma_{C3—C8} \rightarrow \sigma^*_{C9—O10}$ (*t*) is proper of series A. In this case the value of $\delta_{(C3—C8—C9—O10)}$ dihedral angle (95.8°, 92.6°, 109.7° for A^+A^+T, A^+A^-T and G^+A^+T, respectively) accords to a strong overlap between $\sigma_{C3—C8}$ and $\sigma_{C9—O10}$ orbitals in series A and

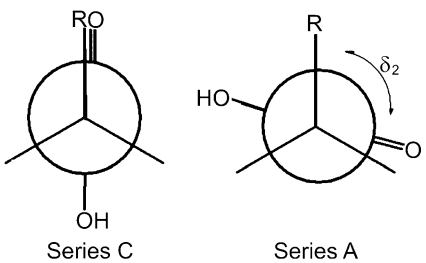

Fig. 3 Scheme of series A and C which one differ in the dihedral angle δ_2

explain the absence of this charge transference in series C ($\delta_{C3—C8—C9—O10}$=0.0° and 16.8° for CCT and A^+CT).

The first 17 transferences shown in Table 5 are higher in CCT explaining their higher stability and it is interesting to analyze some of them in a detailed way. First of all we remark on the $2n_{O10}\rightarrow\sigma^*_{N1—C2}$ transference (0.63 kcal mol^{-1}) that exists only in CCT and can be related to the strongest intramolecular H-bond that characterize the CCT conformer. This charge transference describes the resonance of 2n lone pair of O_{10} oxygen atom with ring A, favored by the planarity of the structure.

Charge delocalizations *c*, *d*, *l, m, q* and *r* involve orbitals of π-symetry: $\sigma_{C—H}\rightarrow\pi^*$ or $\pi\rightarrow\sigma^*_{C—H}$. Their behavior also can be related to F_{ij} term, therefore we can explain better delocalizations through structural factors of molecular geometry. In fact, these delocalizations are related to $\delta_{Hb—C8—C9—O10}$=124.6°, 142.4°, 27.8°, 141.5°, 126.8°, $\delta_{Ha—C8—C9—O10}$=124.7°, 25.4°, 144.8°, 106.2°, 11.2°, $\delta_{C2—C3—C8—Ha}$=122.4°, 125.4°, 136.1°, 123.2°, 165.6°, $\delta_{C2—C3—C8—Hb}$=122.3°, 5.4°, 16.2°, 6.4°, 75.2° for CCT, A^+A^+T, A^+A^-T, A^+CT and G^+A^+T, respectively. We found that dihedral angles larger than 160.0° and less than 28.0° prevent the overlaping between orbitals of σ and π symmetry, and the optimum overlapping occurs at ≈120°.

The $\sigma_{C3a—C3}\rightarrow\sigma^*_{C8—C9}$ delocalization also is explained by augmented F_{ij} and the $\delta_{C3a—C3—C8—C9}$ dihedral angle (180.0°, 65.1°, 77.4°, 66.7° and 134.8° for CCT, A^+A^+T, A^+A^-T, A^+CT and G^+A^+T, respectively) explain the higher value of $E^{(2)}$ in CTT (better overlap: the bonds are antiperiplanar to each other) and also explain why this transference is not found in A^+A^+T, A^+A^-T and A^+CT.

The higher stability (0.19 kcalmol^{-1}) of A^+A^+T with respect to A^+A^-T, cannot be explained through the intermolecular H-Bonds found in both structures, because both of them are similar in strength (Table 4). However, hyperconjugative delocalizations *f*, *g*, *i*, *j*, *k*, *l*, *n*, *o*, *q*, *s*, *t*, *u*, and *w* are stronger in A^+A^+T than in A^+A^-T. Moreover, $\sigma_{C4—H}\rightarrow\sigma^*_{C4—C5}$ delocalization only appears in A^+A^+T.

To explain the higher stability of A^+A^-T with respect to A^+CT (0.26 kcalmol^{-1}) the stabilizing effect of the hydrogen bonding interaction characterized in the first one has to be taken into account.

At this point it is also interesting to deepen the analysis of the hydrogen bonding interactions characterized by AIM. The electronic basis for hydrogen bonding interactions has been analyzed by Alabugin et al. [22], showing that the D—H bond length ("D" is the donor atom) in D—H···A hydrogen bonded complexes is controlled by a balance of two main factors acting in opposite directions: "D—H bond lengthening" due to $n(A)\rightarrow\sigma^*(H—D)$ hyperconjugative interaction balanced by "D—H bond shortening" due to increase in the *s*-character and polarization of the D—H bond. When hyperconjugation dominates, D—H bond elongation is reflected in a concomitant red shift of the corresponding infrared stretching frequency. When the hyperconjugative interaction is weak and the D-hybrid orbital in the D—H bond is able to undergo a sufficient change in hybridization and polarization, rehybridization dominates giving rise to a shortening of the D—H bond and a blue shift in the D—H stretching frequency. Our results showed this behavior in all intramolecular H-bonds. In fact, for the characterized intramolecular H-bonds direct transferences like $n(A)\rightarrow\sigma^*(H—D)$ were not found. Therefore, in all of the conformers rehybridization dominates giving rise to a shortening of the C—H bond. Besides, we found an increase of the *s*-character in carbon-centered hybrid atomic orbital of the C—H bond (Table 6). The increase in *s*-character is a direct consequence of Bent's rules, one of the most general rules governing structure of organic molecules. According to Bent's rule, atomic s character tends to concentrate in orbitals that are directed toward electropositive groups and atomic p character tends to concentrate in orbitals that are directed toward electronegative groups. The decrease in effective electronegativity of hydrogen in a X—H bond giving rise to an increase in the *s*-character of the carbon hybrid orbitals of this bond. Such a decrease in effective electronegativity leads to increased bond polarization (Table 6). This behavior is typical to improper or blue-shifted hydrogen bonding interactions.

Finally, the increased ε values found in the ring A of IAA with respect to Indole can be explained through hyperconjugative charge transferences. In fact in IAA, the second order energy of $\sigma_{C4—C3a}\rightarrow\sigma^*_{C2—C3}$ transference ranges from 0.87 to 0.91 kcalmol^{-1} (Table S2b), (0.66 kcal mol^{-1} in Indole, Table S2a). Besides, the second order energy of $\sigma_{C3a—C7a}\rightarrow\sigma^*_{C3—C8}$ transference ranges from 5.38−5.54 kcalmol^{-1} (3.69 kcalmol^{-1} in Indole). These charge delocalizations explain the reported increase of ε

Table 6 NBO analysis of improper intramolecular H-bonding interactions for IAA monomers at B3LYP/6-31G** level of calculation[a]

Parameters	CTT	A^+A^+T	A^+A^-T	A^+CT	G^+A^+T
qH_2	0.232	0.206	0.208	0.203	0.217
qH_4	0.204	0.223	0.216	0.209	0.205
sp^n (C_2-H)	$sp^{1.96}$	$sp^{2.04}$	$sp^{2.04}$	$sp^{2.05}$	$sp^{2.01}$
% s-char	33.79	32.87	32.92	32.77	33.22
sp^n (C_4-H)	$sp^{2.48}$	$sp^{2.42}$	$sp^{2.44}$	$sp^{2.46}$	$sp^{2.48}$
% s-char	28.69	29.25	29.08	28.85	28.75
Pol (σ_{C2-H}) C%	61.79	60.46	60.57	60.34	61.05
H%	38.21	39.54	39.43	39.66	38.95
Pol (σ_{C4-H}) C%	60.25	61.27	60.87	60.57	60.34
H%	39.75	38.73	39.13	39.43	39.66

[a] Natural charges (q) are expressed in a.u.

values in C_{3a}—C_3 bond in IAA and the consequent increase in their π-character. The increased ellipticity of C_2—C_3 bond is explained by $\sigma_{C2—H} \rightarrow \sigma^*_{C3a—C3}$ charge transference (second order energy ranges from 2.36 to 2.43 kcal mol^{-1} in IAA and is of 2.11 kcal mol^{-1} in Indole, Table S2a) and by $\sigma_{C8—Ha,b} \rightarrow \pi^*_{C2—C3}$ charge transferences (second order energy of 3.25 kcal mol^{-1} on average and only exist in IAA). Therefore, our results show that electron charge delocalization on C_{3a}—C_3 and C_2—C_3 bonds described through those hyperconjugative interactions give rise to the mentioned slight increase of π-character in ring A of IAA with respect to Indole, feature which could be relevant to the radical scavenging activity.

AIM/NBO study of molecular electrostatic potential

Molecular electrostatic potential (MEP) can be useful in understanding sites for electrophilic attack. MEPs are well suited for analyzing processes based on the "recognition" of one molecule by another, as in drug-receptor, and enzyme-substrate interaction, because it is through their potentials that the two species first "see" each other. It is through this potential that a molecule is first "seen" or "felt" by another approaching chemical species, *V*(r) have been used extensively for interpreting and predicting the reactive behavior of a wide variety of chemical systems in both electrophilic and nucleophilic reactions, the study of hydrogen bonding interactions and biological recognition processes [23-32].

The *V*(r), created in the space around a molecule by its nuclei and electrons, have emerged as a useful analytical tool in the study of molecular reactivity. Unlike many of the other quantities used at present and earlier as indices of reactivity, *V*(r), is a real physical property that can be determined experimentally or by computational methods.

However, identification of reactivity patterns based on the MEP exhibits intrinsic drawbacks, since the MEP is obtained through the classical electrostatic potential. Then, it is not possible to determine sites for nucleophilic attack because the zones of positive potential are not necessarily expressing affinity for nucleophiles but the concentrated nature of the nuclear charges. This paper uses the procedure proposed by Politzer et al. [24] for predicting sites targeted for electrophilic attack in the regions of negative *V*(r) values, and NBO and AIM results are reviewed in the light of the complementarities of the different theoretical tools used.

The oxygen atoms of the carboxylic groups are sites that exhibit the highest concentration of charge (Fig. 4). The O10 has a lower negative V(r) (-60.70 kcal mol^{-1}), meanwhile the O11 has a *V*(r) of -37.68 kcal mol^{-1}. Therefore, it is assumed that from all the possible sites, the oxygen atoms will be the preferred ones for an electrophilic attack. The other negative region is associated with N1 (-37.68 kcal mol^{-1}). Thus, our results show that the electron-rich Indole heterocycle and the additional side chain seem to be essential for the radical scavenging. At C5 we also found negative electrostatic potentials (-22.34 kcal mol^{-1}). The latter, indicates activation to electrophilic attack at position 5 in benzenic ring B of IAA; this finding could also be related to their antioxidant properties. Through the analysis of electrostatic potential for Indole at the same level of calculation (Fig. 4) we can conclude that the acetyl moiety have a slight effect on the reactivity toward electrophilic attack of that heterocycle.

In previous works [33, 34] we showed that coordinated analysis of NBO and AIM results allow to rationalize new aspect of the potential created in the space around a molecule. Following the same line of reasoning we found in IAA that the positive *V*(r) values on oxygen atoms that comprise a hydrogen bond (atom of the acceptor moiety) become less negative (higher) than *V*(r) of those that do not comprise it. The positive *V*(r) values on hydrogens atoms of

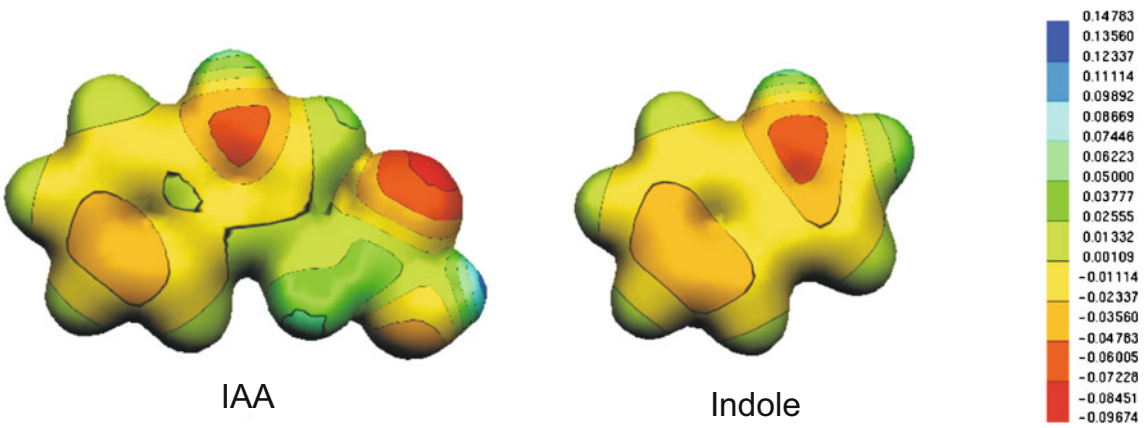

Fig. 4 Maps of molecular electrostatic (MEP) for CCT conformer of IAA and Indole. Values in a.u

the O···H hydrogen bridge (belonging to the donor C—H moiety) become more negative (lower) than the other H of the benzene ring (Fig. 5). Through a AIM/NBO analysis of the MEPs another topic to highlighted is the possibility of characterizing the electrostatic nature of O···H intramolecular weak interactions, and their marked directionality when realizing the asymmetrization of the $V(r)$ distribution on hydrogen and oxygen atoms of the bridge, which is clearly defined by the neighbor oxygen (Fig. 5). Thus, through an AIM/NBO point of view of the MEPs, the analysis of intramolecular O···H hydrogen bonds can be enriched, showing a $V(r)$ value increase on the atom that belongs to the acceptor moiety, while a $V(r)$ value decrease on that of the donor moiety, in agreement with the electrostatic potential complementarity between positive regions of H-donor groups and negative regions of the H-acceptor atom found in intermolecular H-bonds. [35]

Another remarkable aspect is the difference in electrostatic potential values on different hydrogen atoms linked to carbon atoms. As we showed in other compounds in a recent work [33] through the analysis of electrostatic potential on hydrogen atoms of C—H bonds we can anticipate larger donor ability in hyperconjugative transferences associated to those C—H bonds. In IAA the hydrogen attached to C_8 has a higher positive $V(r)$ (23.70 kcalmol^{-1}) than those attached to benzenic ring (8.36 kcalmol^{-1}) (Fig. 6). Correspondingly large hyperconjugative transferences for C—H bond were found (i.e., the second-order stabilization energy of charge transferences from of C_8—H_a bond in CCT is 14.38 kcalmol^{-1} and in A^+A^+T is 10.71 kcalmol^{-1}, see Table S2a). Remarkably, a higher loss of electron charge density on hydrogen atoms in its NCP was found (0.434 a.u. at NCP of $H_{a,b}$ and 0.443 a.u. at NCP of hydrogen H_5 or H_6 in CCT conformer, see Table 7), thus showing the descriptive quality of the electron charge density at nuclear CP and their relationship with MEPs at hydrogen atoms. The donor role of these C—H bonds in hyperconjugative interactions can be related also to their weakening and elongation discussed above. The higher weakening and elongation occurs at C_8—H_a and C_8—H_b of CCT, where the MEP on H is more positive, according to higher charge delocalization (see Table S2a) and consequent higher structural stabilization. In other words, a slight change in MEP can be related to subtle but essential features related to structure stabilization.

With similar arguments we can analyze the behavior of $V(r)$ on H_4 and H_7 (see Fig. 6, Tables S2a and S3)

Conclusions

The conformational space of *1H*-Indole-3-Acetic Acid (IAA) was scanned using molecular dynamics at semiempirical level, and complemented with functional density calculations. We found 14 lowest energy conformers with symmetry C_1, which in stability order are: CCT, A^+A^+T/

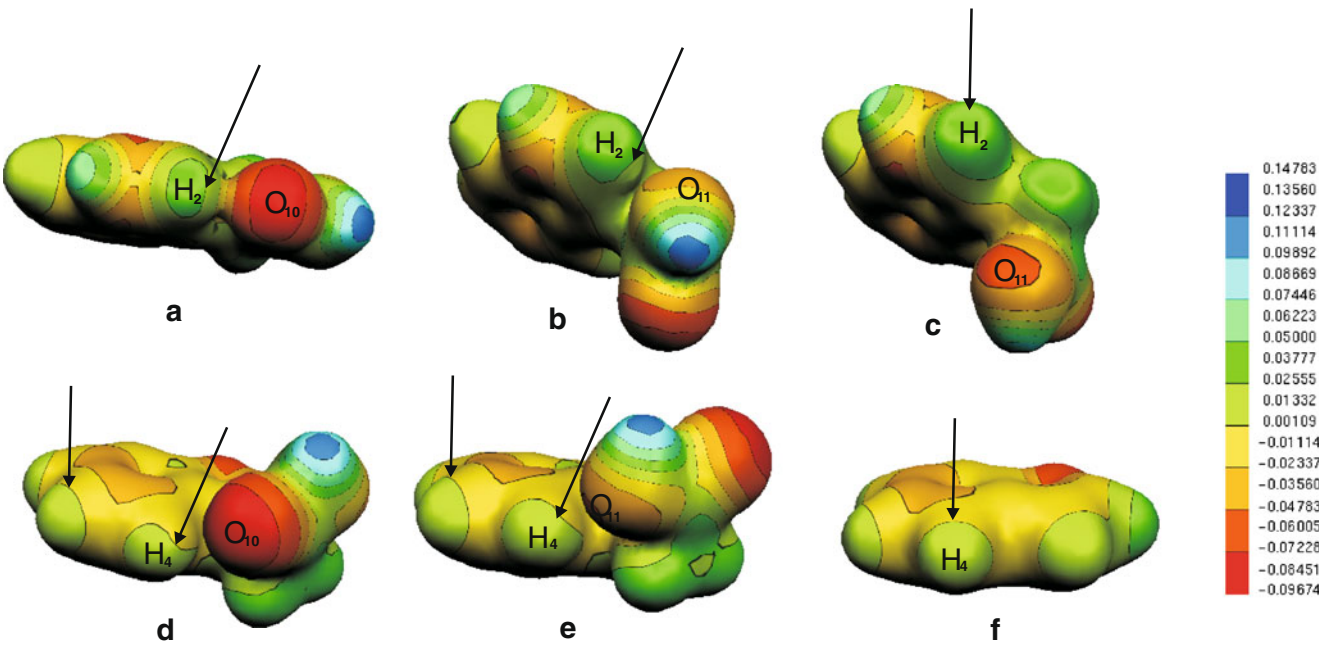

Fig. 5 Maps of molecular electrostatic (MEP) for CCT (**a**), G^+A^+T (**b**), A^+A^+T (**c, d**) and A^+A^-T (**e**) conformers of IAA, and Indole (**f**). Vertical lines indicate hydrogen atoms not involved in any intramolecular H-bond.Oblique lines point out different behavior of $V(r)$ at hydrogen atoms involved in intramolecular H-bond

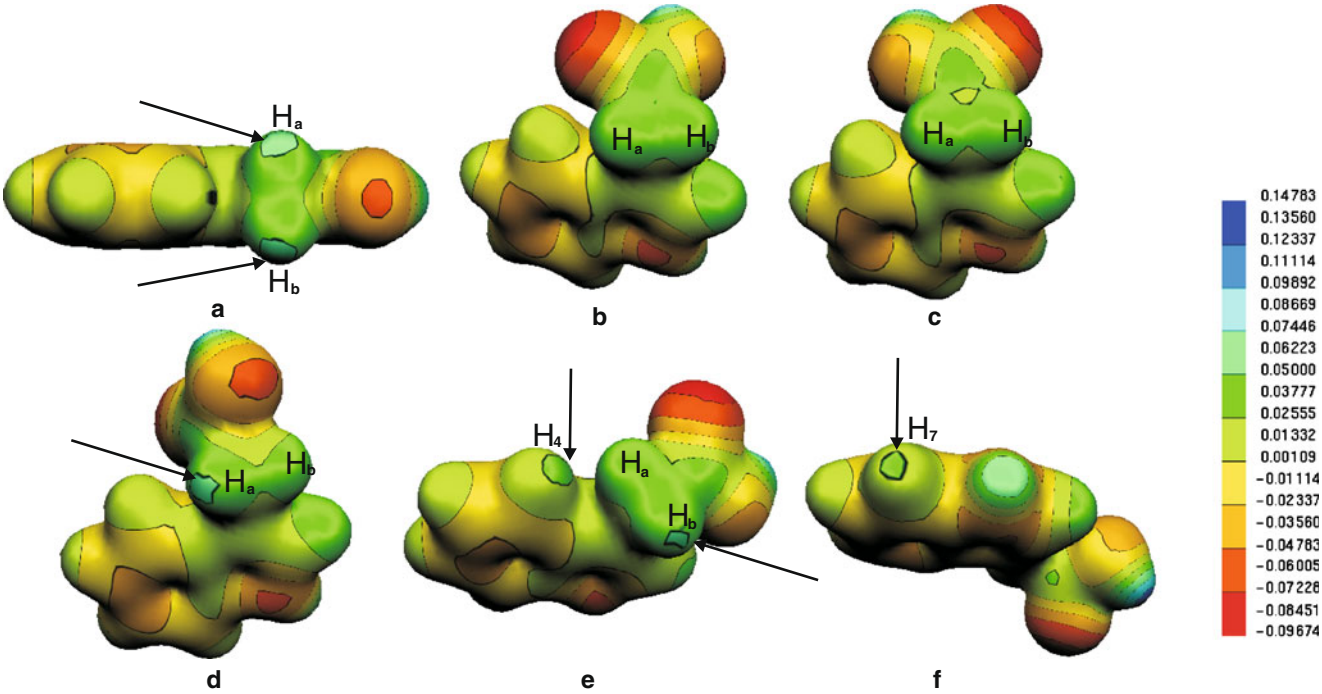

Fig. 6 Maps of molecular elestrostatic potential for CCT (**a**), A^+A^+T (**b**), A^+A^-T (**c**), A^+CT (**d**) and G^+A^+T (**e, f**) conformers of IAA. Obliques lines indicate the increase of $V(r)$ at hydrogen atoms of $C_8H_{(2)}$ moiety. Vertical lines indicate different behavior of $V(r)$ at hydrogen atoms of benzenic ring

A^-A^-T, A^+A^-T/A^-A^+T, A^+CT/A^-CT, G^+A^+T/G^-A^-T, A^+TC/A^-TC, CCC, and A^+CC/A^-CC. Six pairs of them account for structures of the same energy, but differing in the orientation of the acetyl group with respect to the plane of the Indole ring: one of them with the acetyl moiety upward oriented, *Re*-face, and the other isomer having the acetyl moiety downward oriented, *Si*-face.

Through atoms in molecules theory carefull characterization of all intramolecular interactions was done, thus analyzing the effect of the acetyl side chain on the heterocycle proper of Indole thus understanding electronic aspects that could be of fundamental importance in the antioxidant properties of these structures. We conclude that the remarkably effects of the acetyl moiety is the constitution of intramolecular O···H hydrogen bonding interactions. We found two of them related to carbonyl oxygen and another two related to oxygen of OH moiety. Vibrational results and NBO analysis allowed us to draw the conclusion that all of the intramolecular hydrogen bonds found can be classified as improper or blue shifted. The electronic basis for that kind of hydrogen bonding interactions has been profoundly analyzed.

A deep NBO analysis allowed us to explain the stability order of the IAA conformers and the main geometrical and the structural factors that determine better charge delocal-

Table 7 Electron density at nuclear critical points. Values are expressed in a.u

	Atom	Indole	CCT	A^+A^+T	A^+A^-T	A^+CT	G^+A^+T
Ring A	H_1	0.433	0.433	0.433	0.433	0.433	0.433
	H_2	0.439	0.436	0.439	0.439	0.439	0.438
Ring B	H_4	0.441	0.442	0.439	0.441	0.442	0.442
	H_5	0.443	0.443	0.443	0.443	0.443	0.443
	H_6	0.443	0.443	0.443	0.443	0.443	0.443
	H_7	0.440	0.440	0.440	0.440	0.440	0.440
Acetyl moiety	H_a	-	0.434	0.440	0.439	0.433	0.442
	H_b	-	0.434	0.440	0.441	0.438	0.436

ization were discussed. Trough coordinated NBO/AIM analysis subtle effects of acetyl side chain on the reactivity of ring A were shown and the mechanisms underlying the increased π-character of C_2—C_3 and C_{3a}—C_3 bonds were described.

It is additionally noteworthy that the detailed knowledge of the conformational space of the IAA monomer in vacuum, presented herein, was of paramount importance in the study of conformational space of their dimeric forms needed to study IR and Raman spectrum which was done by us in other work [36].

Finally the analysis of MEPs allowed us to describe the reactive sites of the electron-rich Indole heterocycle and the additional acetyl side chain. Moreover through NBO and AIM results we show that MEPs are not only useful for predicting sites targeted for electrophilic attack in IAA but also could show subtle but essential features related also with intramolecular weak interactions, charge delocalization and structure stabilization.

Acknowledgments Thanks are due to Agencia de Promoción Científica y Tecnológica Argentina (MINCYT), CONICET and Universidad Nacional de La Plata (Argentina) for financial support. A.H.J. is Member of the Scientific Research Career (CIC, Provincia de Buenos Aires). A.A.V. is a Research Member of the National Research Council of Argentina (CONICET). M.C.P.S. acknowledges a fellowship (IP-PRH N^0 54) from Agencia de Promoción Científica y Tecnológica Argentina and Universidad de la Cuenca del Plata (Corrientes, Argentina) and R.M.L. acknowledges Universidad de la Cuenca del Plata for facilities provided during the course of this work.

References

1. Reiter RJ, Tan DX, Terron MP, Flores LJ, Czarnocki Z (2007) Melatonin and its metabolites: New findings regarding their production and their radical scavenging actions. Acta Biochim Pol 54:1-9
2. Khan MTH (2007) Bioactive Heterocycles V. Springer,Berlin, pp 145-154
3. Bozkaya P, Dogan B, Suzen S, Nebioglu D, Ozkan SA (2006) Determination and investigation of electrochemical behaviour of 2-phenylindole derivatives: Discussion on possible mechanistic pathways. Can J Anal Sci Spectrosc 51:125-139
4. Kruk I, Aboul-Enein HY, Michalska T, Lichszteld K, Kubasik-Kladna K, Olgen S (2007) *In vitro* scavenging activity for reactive oxygen species by *N*-substituted indole-2-carboxylic acid esters. J Lumin 22:379-386
5. Shirinzadeh H, Eren B, Gurer-Orhan H, Suzen S, Özden S (2010) Novel Indole-Based Analogs of Melatonin:Synthesis and *in vitro* Antioxidant Activity Studies. Molecules 15:2187-2202
6. Poeggeler B, Thuermann S, Dose A, Schoenke M, Burkhardt S, Hardeland R (2002) Melatonin's unique radical scavenging properties - roles of its functional substituents as revealed by a comparison with its structural analogs. J Pineal Res 33:20-30
7. Bader RFW (1995) Atoms in molecules. A quantum theory. Oxford University Press, Oxford
8. Popelier P (2000) Atoms in molecules. An introduction. Prentice Hall
9. Bader RFW (1990) A quantum theory of molecular structure and its applications. Chem Rev 91:893-928
10. Glendening ED, Reed AE, Carpenter JE, Weinhold F NBO 3.1. (2003) Program as implemented in the Gaussian 03 package
11. HyperChem Release 7.5, Hypercube Inc, USA
12. Frisch MJ, Trucks GW, Schlegel HB, Scuseria GE, Robb MA, Cheeseman JR, Montgomery JA Jr, Vreven T, Kudin KN, Burant JC, Millam JM, Iyengar SS, Tomasi J, Barone V, Mennucci B, Cossi M, Scalmani G, Rega N, Petersson GA, Nakatsuji H, Hada M, Ehara M, Toyota K, Fukuda R, Hasegawa J, Ishida M, Nakajima T, Honda Y, Kitao O, Nakai H, Klene M, Li X, Knox JE, Hratchian HP, Cross JB, Adamo C, Jaramillo J, Gomperts R, Stratmann RE, Yazyev O, AJ Austin, Cammi R, Pomelli C, Ochterski JW, Ayala PY, Morokuma K, Voth GA, Salvador P, Dannenberg JJ, Zakrzewski VG, Dapprich S, Daniels AD, Strain MC, Farkas O, Malick DK, Rabuck AD, Raghavachari K, Foresman JB, Ortiz JV, Cui Q, Baboul AG, Clifford S, Cioslowski J, Stefanov BB, Liu G, Liashenko A, Piskorz P, Komaromi I, Martin RL, Fox DJ, Keith T, Al- Laham MA, Peng CY, Nanayakkara A, Challacombe M, Gill PMW, Johnson B, Chen W, Wong MW, Gonzalez C, Pople JA (2003) Gaussian03, Revision B.02. Gaussian Inc; Pittsburgh PA
13. Becke AD (1993) Density-functional thermochemistry. III. The role of exact exchange. J Chem Phys 98:5648-5652
14. Lee C, Yang W, Parr RG (1988) Development of the Colle-Salvetti correlation energy formula into a functional of the electron density. Phys Rev B 37:785-789
15. Biegler-König FW, Bader RFW, Tang TH (1982) Calculation of the average properties of atoms in molecules. II. J Comput Chem 3:317-328
16. Flúrkiger P, Lúthi HP, Portmann S, Weber J (2000) MOLEKEL 4.0. Swiss Center for Scientific Computing, Manno, Switzerland
17. Chemistry, IUPAC, Rules for the Nomenclature of Organic Chemistry, Section E Stereochemistry (1976) Pure Appl Chem 45:11
18. Gilli G, Gilli P (2009) The Nature of the Hydrogen Bond. Oxford University Press, USA
19. Bader RFW (1998) A Bond Path: a universal indicator of bonded interactions. J Phys Chem A 102:7314-7323
20. Cremer D, Kraka E, Slee TS, Bader RFW, Lau CDH, Nguyen-Dang TT, MacDougall PJ (1983) Description of homoaromaticity in terms of electron distributions. J Am Chem Soc 105:5069
21. Hobza P, Havlas Z (2000) Blue-Shifting Hydrogen Bonds. Chem Rev 100:4253-4264
22. Alabugin IV, Manoharan M, Peabody S, Weinhold F (2003) Electronic Basis of Improper Hydrogen Bonding: A Subtle Balance of Hyperconjugation and Rehybridization. J Am Chem Soc 125:5973-5987
23. Scrocco E, Tomasi J (1978) Electronic molecular structure, reactivity and intermolecular forces: an euristic interpretation by means of electrostatic molecular potentials. Adv Quantum Chem 11:115-193
24. Politzer P, Truhlar DG (eds) (1981) Chemical applications of atomic and molecular electrostatic potentials. Plenum, NY
25. Politzer P, Landry SJ, Warnheim T (1982) Proposed procedure for using electrostatic potentials to predict and interpret nucleophilic processes. J Phys Chem 86:4767-4771
26. Politzer P, Abrahmsen L, Sjoberg P (1984) Effects of amino and nitro substituents upon the electrostatic potential of an aromatic ring. J Am Chem Soc 106:855-860

27. Politzer P, Laurence PR, Jayasuriya K (1985) Molecular electrostatic potentials: an effective tool for the elucidation of biochemical phenomena. Environ Health Perspect 61:191-202
28. Politzer P, Murray JS (1991) Theoretical biochemistry and molecular biophysics: a comprehensive survey, vol 2. In: Beveridge DL, Lavery R (eds) Protein. Adenine, Schenectady, pp 165-191
29. Murray JS, Lane P, Brinck T, Politzer P, Sjoberg P (1991) Electrostatic potentials on the molecular surfaces of cyclic ureides. J Phys Chem 95:844-848
30. Muñoz-Caro C, Niño A, Sement ML, Leal JM, Ibeas S (2000) Modeling of protonation processes in acetohydroxamic acid. J Org Chem 65:405-410
31. Politzer P, Murray J, Concha MC (2002) The complementary roles of molecular surface electrostatic potentials and average local ionization energies with respect to electrophilic processes. Int J Quantum Chem 88:19-27
32. Roy DK, Balanarayan P, Gadre SR (2009) Signatures of molecular recognition from the topography of electrostatic potential. J Chem Sci 121:815-821
33. Lobayan RM, Jubert AH, Pomilio AB (2009) Conformational and electronic (AIM/NBO) study of unsubstituted A-type dimeric Proanthocyanidin. J Mol Model 15:537-550
34. Bentz E, Jubert AH, Pomilio AB Lobayan RM (2010) Theoretical study of Z isomers of A-type dimeric proanthocyanidins substituted with R=H, OH and OCH3. Stability and reactivity properties. J Mol Model. doi:10.1007/s00894-010-0682-z
35. Pacios LF (2006) Chapter 3: Changes of Electron Properties in the Formation of Hydrogen Bonds. In: Grabowski SJ (ed) Hydrogen Bonding-New Insights. Springer,Berlin
36. Pérez Schmit MC, Jubert AH, Vitale A, Lobayan RM (2010) Theoretical studies and vibrational spectra of 1 H-Indole-3-Acetic Acid conformers. Exploratory conformational analysis of dimeric species. Submitted.